Geomechanics and Engineering, *Vol. 18, No. 4 (2019) 353-362*
DOI: https://doi.org/10.12989/gae.2019.18.4.353

Water-induced changes in mechanical parameters of soil-rock mixture and their effect on talus slope stability

Haofeng Xing*[1], Liangliang Liu[1a] and Yong Luo[2b]

[1]Department of Geotechnical Engineering, Tongji University, Shanghai 200092, China
[2]Department of Geology Survey and Design,
Guizhou Transportation Planning Survey and Design Academe Co., Ltd., Guiyang, 550001, China

(Received December 26, 2018, Revised May 19, 2019, Accepted June 15, 2019)

Abstract. Soil-rock mixture (S-RM) is an inhomogeneous geomaterial that is widely encountered in nature. The mechanical and physical properties of S-RM are important factors contributing towards different deformation characteristics and unstable modes of the talus slope. In this paper, the equivalent substitution method was employed for the preparation of S-RM test samples, and large-scale triaxial laboratory tests were conducted to investigate their mechanical parameters by varying the water content and confining pressure. Additionally, a simplified geological model based on the finite element method was established to compare the stability of talus slopes with different strength parameters and in different excavation and support processes. The results showed that the S-RM samples exhibit slight strain softening and strain hardening under low and high water content, respectively. The water content of S-RM also had an effect on decreasing strength parameters, with the decrease in magnitude of the cohesive force and internal friction angle being mainly influenced by the low and high water content, respectively. The stability of talus slope decreased with a decrease in the cohesion force and internal friction angle, thereby creating a new shallow slip surface. Since the excavation of toe of the slope for road construction can easily cause a landslide, anti-slide piles can be used to effectively improve the slope stability, especially for shallow excavations. But the efficacy of anti-slide piles gradually decreases with increasing water content. This paper can act as a reference for the selection of strength parameters of S-RM and provide an analysis of the instability of the talus slope.

Keywords: soil-rock mixture; triaxial test; water content; strength parameter; talus slope; slope stability

1. Introduction

A soil-rock mixture (S-RM) is a special type of inhomogeneous geomaterial which was formed in the quaternary era and is a geological body existing abundantly in nature (Xu *et al*. 2008, Brandes *et al*. 2011, Wang and Li 2014, Huang *et al*. 2015, Cen *et al*. 2017), especially in mountainous areas. It consists of both soil particles having relatively weak strength and very strong irregular rock blocks of various sizes (Zhang *et al*. 2016, Tan *et al*. 2016, Wang *et al*. 2017). Due to the particle size and arrangement mode within rock blocks, and the distribution ratio and cementation form of rock blocks and the soil, the physical and mechanical properties of the S-RM are significantly different when compared to that of pure soil or rock. Moreover, since S-RM landslides have become major geological disasters in the recent past (Xu *et al*. 2011, Sun *et al*. 2014), this research topic is very relevant to the field of geomechanics (Vallejo 2001, Xu *et al*. 2007, Li *et al*. 2016).

Talus slopes are widely distributed across the southwest mountain area of China, with their surface soil layer being normally comprised of S-RM. Due to the loose structure of S-RM, the talus slope is vulnerable to collapse when under the influence of external forces such as rainfall, earthquake and excavations (Sun *et al*. 2014, Kanungo *et al*. 2013, Wang *et al*. 2014, Anbazhagan *et al*. 2017, Liu *et al*. 2017, Moradi *et al*. 2018). Since the instability of talus slopes can lead to huge economic losses, it is very important to study their stability in order to avoid landslides (Liu *et al*. 2009, Mohammadi and Taiebat 2016). Also, the construction and extensions of expressways has penetrated deeper into the mountains in the 21st century, inevitably involving the excavation and support of the talus slope and in turn, gradually unveiling the features and problems associated with S-RM.

S-RM possesses shear strength parameters which exhibit complex mechanical characteristics due to the complicated nature of its components (Chang and Phantachang 2016, Dimitrova and Yanful 2012). It is essential to select the proper shear strength parameters during the study of the talus slope stability. Many researchers have conducted laboratory and field tests that employ a variety of methods to analyze the physical and mechanical properties of S-RM and talus slope.

These researchers have studied the influence of content and distribution of rock blocks on strength and deformation

*Corresponding author, Associate Professor
E-mail: hfxing@tongji.edu.cn
[a]Ph.D. Student
E-mail: liuliangliang@tongji.edu.cn
[b]Ph.D.
E-mail: 2280130169@qq.com

http://www.techno-press.org/?journal=gae&subpage=7
ISSN: 2005-307X (Print), 2092-6219 (Online)

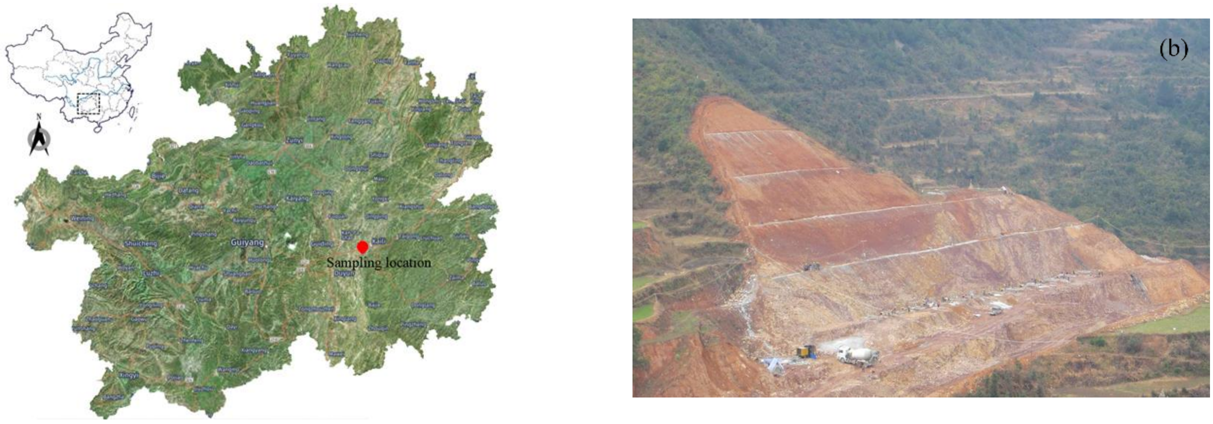

Fig. 1 Geographical location of sample region (a) and the whole Xiaomiaoling talus slope groups (b)

on both the macro and micro scales. However, conventional laboratory tests (such as fall cone test, direct shear test, conventional triaxial test and radial-splitting test) are restricted by the size of the particle and thus cannot replicate the effect of coarse particles very well (Cabalar and Mustafa 2015, Xu *et al*. 2015, Fei 2016). Also, determining the mechanical properties of S-RM requires the use of large loading systems that can simulate actual stress states, which is difficult to replicate in a traditional laboratory test (Vallejo and Mawby 2000). Field tests ensure that the original internal structural characteristics of S-RM and field stress conditions are maintained. But the spatial distribution of the coarse particles in natural S-RM is random, causing the strength parameters obtained from field tests to also be variable (Xu *et al*. 2011, Cen *et al*. 2017). Also, since the selection of cross section of S-RM varies based on image processing technology, it results in uncertainty in generating the S-RM model.

Furthermore, the aforementioned studies almost completely focus on the internal factors (e.g., coarse particle content, weight proportion, size distribution etc.) to analyze the structural and mechanical characteristics of S-RM. It is clear that few reports have been published about the effects of external conditions (e.g., rainfall, earthquake, human factor etc.) on S-RM properties and talus slope stability. And at present there is little research on the mechanical parameters of S-RM sampled from natural sliding mass based on large-scale triaxial test. In addition, the natural and geological environment of talus slope are unique and the defined strength parameters must be applied to the corresponding talus slope to analyze the stability, which is rarely mentioned.

In this paper, the S-RM are sampled from the sliding mass of Xiaomiaoling. It uses large-scale indoor triaxial tests to investigate the influence of water content on strength characteristics of S-RM, which minimizes the restrictions of coarse particle size. The simplified geological model based on finite element method is established on the basis of real terrain. It can compare the stability of talus slope at different strength parameters and in different excavation and support process. The presented results contribute towards the understanding of shear strength characteristics and failure mechanism of S-RM and evaluate the stability of talus slope in excavation support.

2. Preparation of test sample

2.1 The test material

The S-RM sample was obtained from Xiaomiaoling talus slope groups along the Kai-Yang expressway in the Guizhou province of China (Fig. 1(a)). The width of the slope's front edge is about 260 m and the maximum plane length is 250 m. The maximum depth of sliding surface is 35.5 m and the volume is about 8.2×10^5 m^3. The maximum diameter of the rock block in S-RM is up to 1 m and is filled with silty clay or argillaceous silt (Fig. 1(b)). Due to the uneven distribution of S-RM, the samples were taken from different regions and depths.

The talus deposits of Xiaomiaoling area are quaternary deposits and thus, exhibit strong biological and chemical weathering. Clay mineral can also be commonly found in rock debris. As seen in Fig. 2, the obtained samples exhibit rich gradation. The particles have various shapes, most of which are angular and sub-angular with bad psephicity. The sizes of the majority of rock blocks range from 0.5 to 10 cm, with 15 cm being the maximum size. The large particle size gravels are mainly S2w sandstone and some of them are extremely weathered.

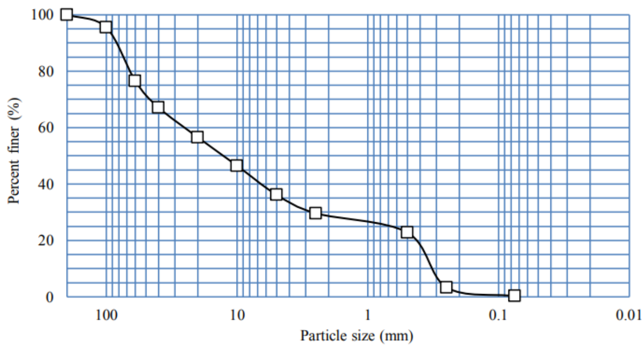

Fig. 2 Gradation curve of the soil-rock mixture material

Table 1 Particle gradation of original sample

Particle size range (mm)	>60	60-40	40-20	20-10	10-5	5-2.5	2.5-0.5	0.5-0.075	<0.075
Content (%)	23.5	9.4	10.6	10.1	10.3	6.6	6.8	16.3	6.4

Table 2 Particle gradation of sample after equivalent substitution

Particle size range (mm)	60-40	40-20	20-10	10-5	5-2.5	2.5-0.5	0.5-0.075	<0.075
Content (%)	14.9	16.7	16.0	16.3	6.6	6.8	16.3	6.4

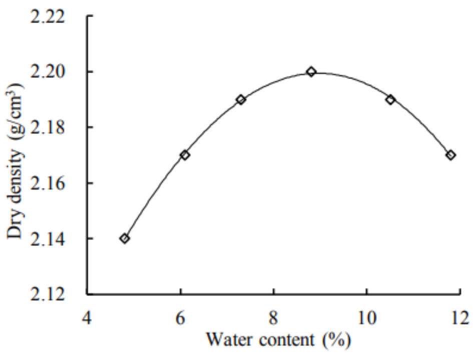

Fig. 3 The compacting curve of S-RM

2.2 The treatment of oversized particles

In the study of the engineering and mechanical properties of S-RM, it is often necessary to use large instruments to perform tests because of the large particle size (Wang *et al*. 2015, Zhong *et al*. 2016, Zhou *et al*. 2018). For the large-scale triaxial test, the most frequently used specimen size is 300 mm in diameter and 600~700 mm in height, and the maximum allowable size of particles is 60 mm. However, the maximum particle size of a rock block in S-RM is usually more than 60 mm, even going as high as 1000 mm in the studied region, which far exceeds the maximum allowed value of the test instrument. Accordingly, the equivalent substitution method has been employed to reduce the scale effect of the oversized particles as it is generally suitable for particles with less than 50% of the largest size (Huang *et al*. 2015, Zhang *et al*. 2016a, b).

The oversized particles in S-RM were replaced by coarse particles with sizes determined by the weighted average method, ranging from the maximum allowable particle size (d_{max} = 60 mm) to 5 mm. Additionally, the particle content of the replaceable particle size shall be calculated using Eqs. (1) and (2).

$$P_i = \frac{P_{0i}}{P_5 - P_0} P_0 + P_{0i} \tag{1}$$

$$P_5 = \sum_{1}^{n} P_{0i} + P_0 = \sum_{1}^{n} P_i \tag{2}$$

where P_5 is the coarse material content (d >5 mm); P_{0i} is the particle content of a certain group with $5 < d < 60$ mm before treatment; P_i is the particle content corresponding to P_{0i} after treatment; and P_0 is the oversized particle content (d > 60 mm).

In this experiment, the percentage content of fine sand in S-RM is relatively higher, whereas that of oversized particles is only 23.5%. The gradation of samples in triaxial test can be seen in Tables 1 and 2.

According to the Chinese professional standard for coarse-grained soil tests (DL/T5356, 2006), the maximum diameter of the compaction test apparatus is 300 mm, which is suitable for soil with a diameter less than 60 mm. Thus, the equivalent substitution method is used once again in the compaction test. The compacting properties of S-RM are studied based on the results of the heavy compaction test. The compression must be performed three times for each test and the compaction energy is 2690 kJ/m^3. From the compaction curve (Fig. 3), the maximum dry density of the mixtures is 2.20 g/cm^3 and the optimum water content is about 8.8%. The curve shows that the dry density increases with an increase in water content up to a certain limit, beyond which the dry density decreases. This phenomenon is similar to that observed in cohesive soils (Butalia *et al*. 2003). For cohesive soils, when the water content is above the optimum level, the soils are considered to be approximately saturated. But the S-RM sample with complex composition has the properties of both rock blocks and fine grained soil, which makes this problem more complicated (Zhong *et al*. 2016, Wang *et al*. 2017). In these experiments, the samples with different percentages of water content are all unsaturated.

3. Test method and procedure

The static-dynamic triaxial apparatus STX-600 manufactured by the Geotechnical Consulting & Testing System is used to carry out this experiment. The diameter of the sample is 300 mm, the constrained diameter of the instrument is 60 mm, the maximum axial force provided by the load frame is 1000 kN and the triaxial pressure cell can withstand pressures up to 2 MPa. The universal digital signal conditioning control unit, which is connected to the computer to enable complete control of data gathering and its functions, has been applied for storing data and digital input/output. The built-in CATS software can eliminate the complex computation process of the program design procedure with the help of calculated test parameters (Fig. 4). And according to the data collected, the software can automatically correct the sectional area of specimen and output accurate deviator stress and strain in real time.

In the case of rapid excavation where talus slope with poor permeability is created, the water in the pores is not easily discharged and the coarse-grained soil has not achieved complete consolidation. Hence, it is more reasonable to conduct unconsolidated undrained triaxial tests using samples having different percentages of water content, which is suitable for the stability analysis of talus slope that is described in the second part of this study. The soil samples are then weighed and experimental criteria such as the dry density and sample size are calculated, after which the prepared soil samples with different particle sizes are evenly blended. Then six layers of the samples are filled and compacted. The samples are cylindrical in shape with a diameter of 300 mm and height of 600 mm. To prevent rubber membrane from being punctured, it is necessary to check whether the rubber membrane leaks before and after experiment. Meanwhile, two stainless steel O-rings tightly hold the rubber membrane on the outside sides of pedestal and top-cap to prevent water seepage from the top and bottom. Some of the experimental parameters are shown in Table 3.

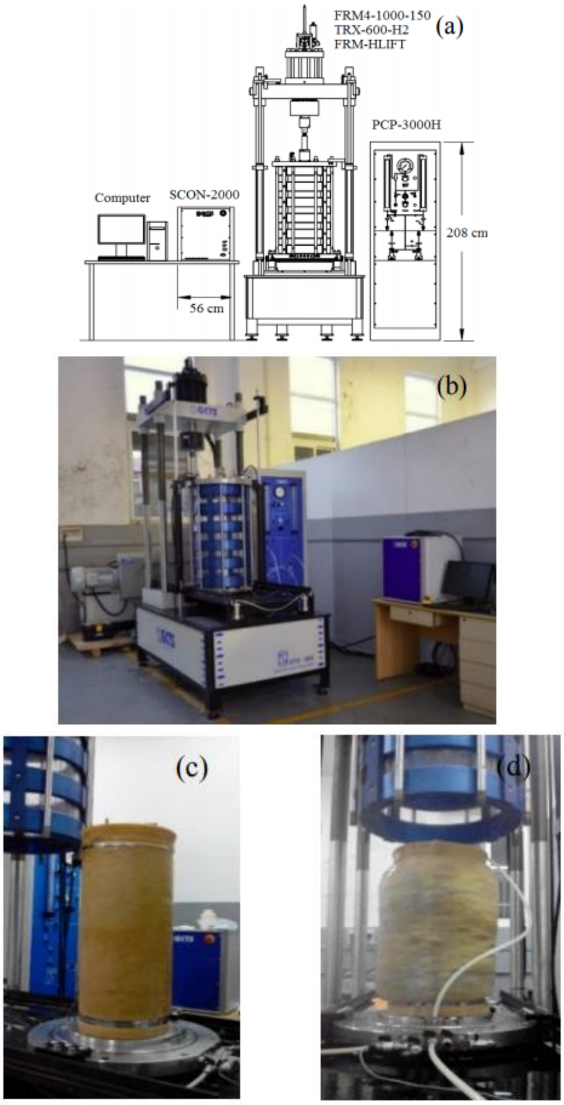

Fig. 4 Large-scale triaxial test performed in laboratory: (a) schematic diagram of instrument, (b) photograph of instrument, (c) test sample of S-RM and (d) failure mode of S-RM

Table 3 Some experimental parameters of large-scale triaxial test scheme

Parameter	Value
Water content (%)	0/5/10/15
Confining pressure (kPa)	100/200/400
Dry density (g/cm^3)	2.0
Loading rate (mm/min)	1.2
Strain threshold (%)	15

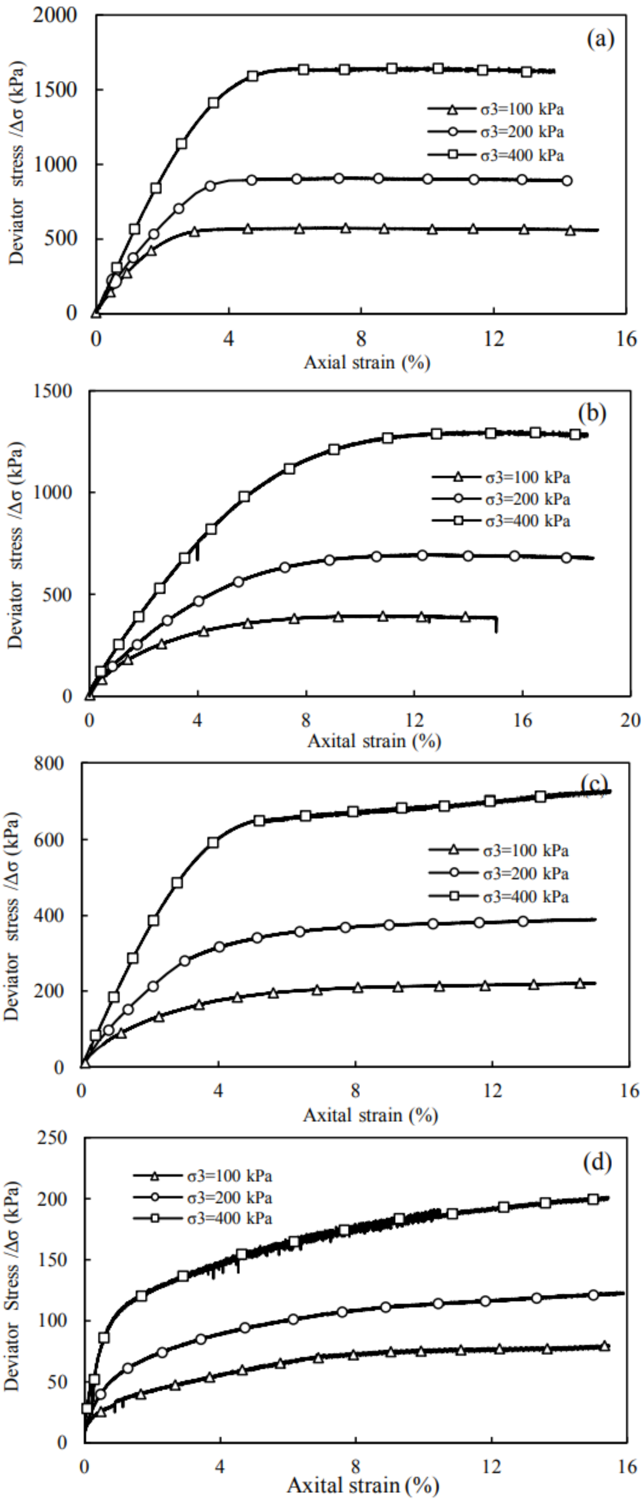

Fig. 5 Deviator stress to axial strain curve under different percentages of water content (a-d corresponds to water content 0%, 5%, 10%, 15%, respectively)

4. Test results and analysis

4.1 Analysis of stress and strain characteristics

Large-scale unconsolidated undrained triaxial tests are performed on the prepared samples with four different percentages of water content. The deviator stress to axial strain curves under different confining pressures are then obtained, which can be seen in Fig. 5.

As shown in Fig. 5, the stress-strain curve is a typical non-linear relationship. When the samples are compressed to a certain degree, the first two sample groups exhibit slight strain softening and the variations between the peak values and stability values of deviator stress are relatively small, whereas the last two sample groups demonstrate

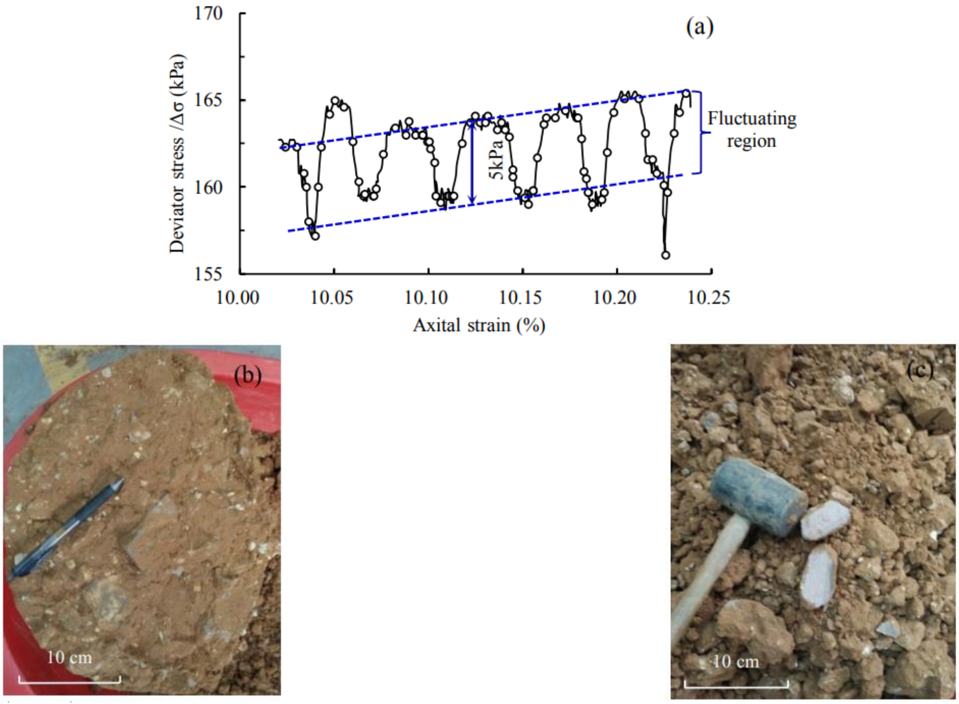

Fig. 6 The partial stress-strain curve of sample with 15% water content (a) and particle breakage of sample with 5% water content (b), (c)

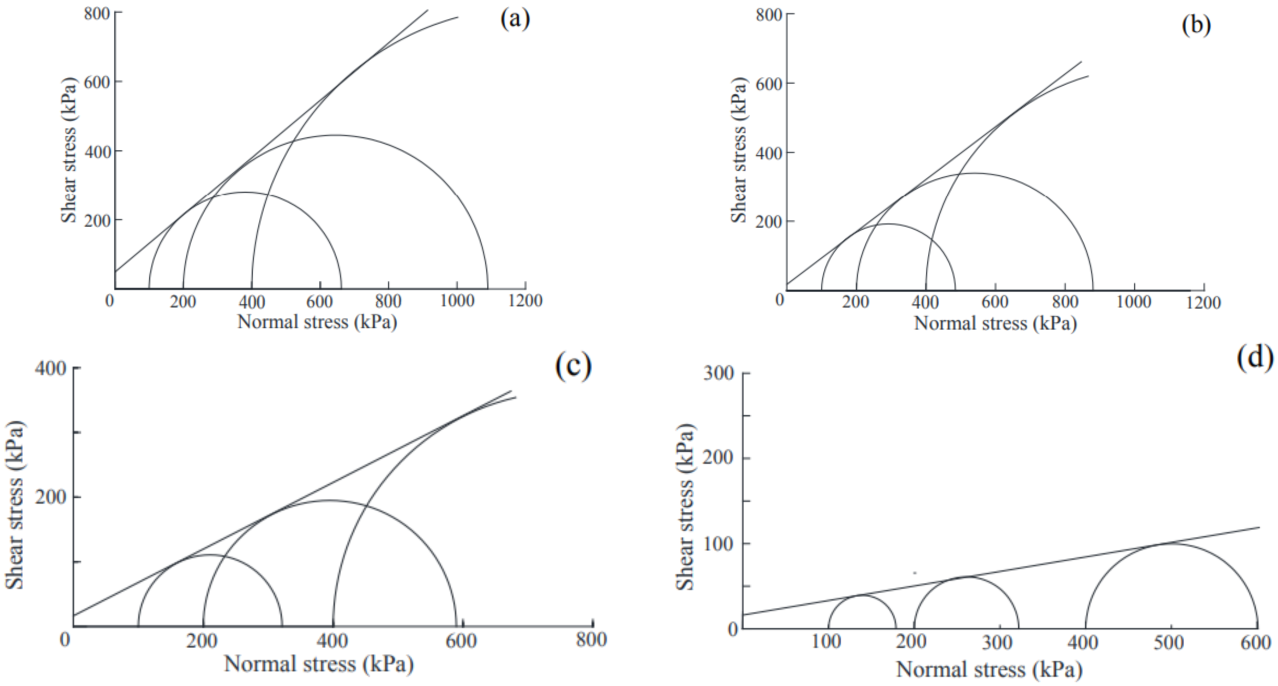

Fig. 7 Mohr circle and strength envelope line based on the Mohr-Coulomb strength theory at different percentages of water content (a-d corresponds to water content 0%, 5%, 10%, and 15% respectively)

Table 4 Shear strength parameter values based on Mohr Coulomb strength theory

Groups	Water content (%)	Cohesive force (kPa)	Internal friction angle (°)
a	0	48.8	39.6
b	5	17.9	37.2
c	10	16.5	27.3
d	15	16.1	10.2

strain hardening effect. This indicates that the S-RM has remarkable plastic deformation features. However, the strain softening resulting from high density of the sample is less significant when compared to that of compact fine grained soil, and the S-RM samples can still withstand greater stress after reaching peak strength.

Under a low confining pressure, the curve is relatively flat with minor fluctuations. However, local fluctuations can be observed under high confining pressure, particularly, in the sample with 15% water content. Within the loading range, the stress continues to increase in the case of high water content, which also demonstrates some strain hardening behaviour. The strengths of samples with different percentages of water content vary greatly under the same confining pressure. The samples with high water content do not exhibit the weak strength-softening phenomenon and the strength always increases within the loading range. The amplitude of decrease in strength gradually reduces after the strain reaches 10%.

The stress-strain curve obtained from the test is not smooth and a partial fluctuation is still observed. For e.g., when the water content of sample is 15% and the strain is in the vicinity of 10%, the local fluctuation of strength appears to be between 155 kPa-165 kPa, as shown in Fig. 6(a). While this phenomenon is also observed in the other three groups, the overall trend of the curve is still uniform. The fluctuations of the curve occur mainly due to the fact that the strength of S-RM is provided by the skeleton of coarse particles and the point contact is mostly between the particles. Also, the local stress exceeds the contact strength of particles in the shear process, which causes cusp breakage or particle breakage and then leads to the fluctuation of stress and strain (Fig. 6(b), 6(c)). Finally, particles are rearranged under pressure to continue to create a new equilibrium state.

4.2 Shear strength analysis

The strength envelope lines are observed to be typically linear under the confining pressures of 100 kPa, 200 kPa and 400 kPa. The Mohr-Coulomb failure criterion has been introduced to determine the shear strength parameters c and φ. The variation of shear strength parameters c and φ at different percentages of water content are plotted in Fig. 7 and listed in Table 4.

With an increase in the water content of the sample, there is a general decrease in the strength parameters of S-RM, which indicates that the water has a softening effect on coarse-grained particles. In the deformation and failure process of the talus slope, the water will enter the soil particles along a joint or fissure plane, resulting in a softening of the original surface structure. The comparison of the first two groups of samples indicates that the cohesion force decreases significantly (by more than 50%) but there is little change in the internal friction angle due to the influence of water. When the water content is high (the last two tested groups having 10% and 15% water content), the result is reversed, but there is still a visible reduction in both the cohesive force and the internal friction angle.

The presence of water decreases the roughness of coarse grained soil and the friction force of sliding and rolling between particles. Water also leads to the softening and disintegration of “mud”, which displays greater strength and cementation, and reduces the occlusal effect between particles which in turn reduces the material strength parameters.

This study demonstrates that there are two limited types of water content, namely, the low limit water content and high limit water content, which influence the cohesive force and internal friction angle at different levels. The main influence of the low limit water content can be observed on the cohesive force, i.e., when the water content is less than the low limit content, the decrease in the magnitude of the cohesive force becomes greater as the water content increases. But when the water content is more than the low limit content (about 0%~5% in this experiment), the decrease in magnitude is not large. The effect of the high limit water content on the reduction of strength parameters can be mainly observed with respect to the internal friction angle. The decrease in magnitude of the internal friction angle is stable before the water content reaches the high limit content (about 10% ~ 15%). After that, the decrease in magnitude increases rapidly with an increase in water content. Generally, the decrease in S-RM strength is largely due to the change in cohesive force at low water content and the change in internal friction angle at high water content.

5. Stability analysis of talus slope

5.1 Establishment of simplified geological model

The composition and origin of the different types of accumulated bodies in talus is quite complicated. In this paper, the talus slope mainly includes S-RM, colluvial-rubble soil, strong weathered sandstone and bedrock. The respective physical and mechanical parameters of soil layers were obtained using laboratory testing, field investigation and engineering concepts. The model created by combining the contents of S-RM and colluvial-rubble soil is the Mohr–Coulomb model. The calculated physical and mechanical parameters for the soil layers of the Xiaomiaoling talus slope were selected during the numerical test, as shown in Table 5.

The experimental process for the model was simulated using the PLAXIS 2D (version 8.5) software and was based on the finite element method to analyze the stability of talus slope during excavation by using different shear strength parameters of S-RM. The two-dimensional calculation models were created based on a typical engineering geological section of the talus slope, and the stratification and nomenclature of soil layers has been shown in Fig. 8. For the boundary conditions, the surface of the talus slope is assumed to be the free boundary condition and the bottom boundary is completely fixed along the vertical direction, while there is no horizontal displacement at both the left and the right vertical boundaries. Additionally, all the boundary conditions of displacement constraints for the numerical model are rigid.

5.2 Global stability analysis of talus slope

In this case, the excavation and support of the talus slope are not taken into account. Different percentages of water content correspond to different shear strength parameters (i.e., cohesive force and internal friction angle) of S-RM, and this section only considers the influence of water content on the global stability of talus slope. Also, since the silt content of fine grained soil in S-RM is relatively high and its surface permeability is poor, varying the strength parameters of S-RM provides a method to

Table 5 Physico-mechanical parameters adopted for the numerical simulation of talus slope

Soil types	Natural density (kg/m^3)	Saturation density (kg/m^3)	Elastic Modulus (MPa)	Poisson ratio	Cohesive force (kPa)	Internal friction angle (°)
S-RM	2000	2100	40	0.20	48.8/17.9 16.5/16.1	39.6/37.2 27.3/10.2
Colluvial-rubble soil	2200	2300	45	0.25	20	32
Strong weathered sandstone	2300	2400	1000	0.28	60	30.5
Bedrock	2500	2700	40000	0.26	27000	43

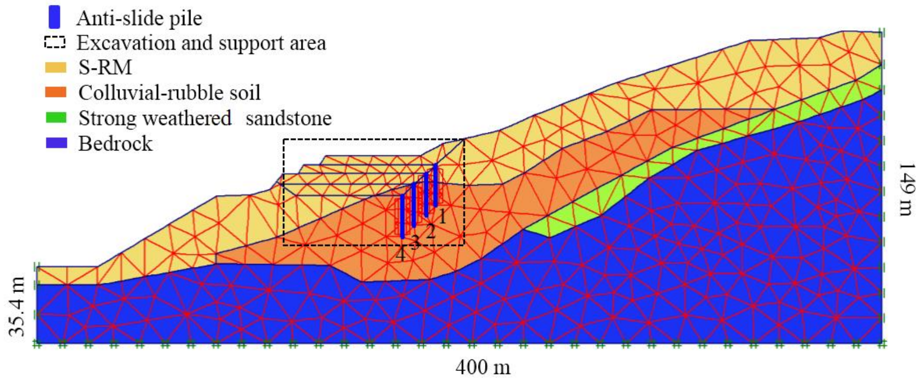

Fig. 8 Simplified soil layers and partition names of talus slope

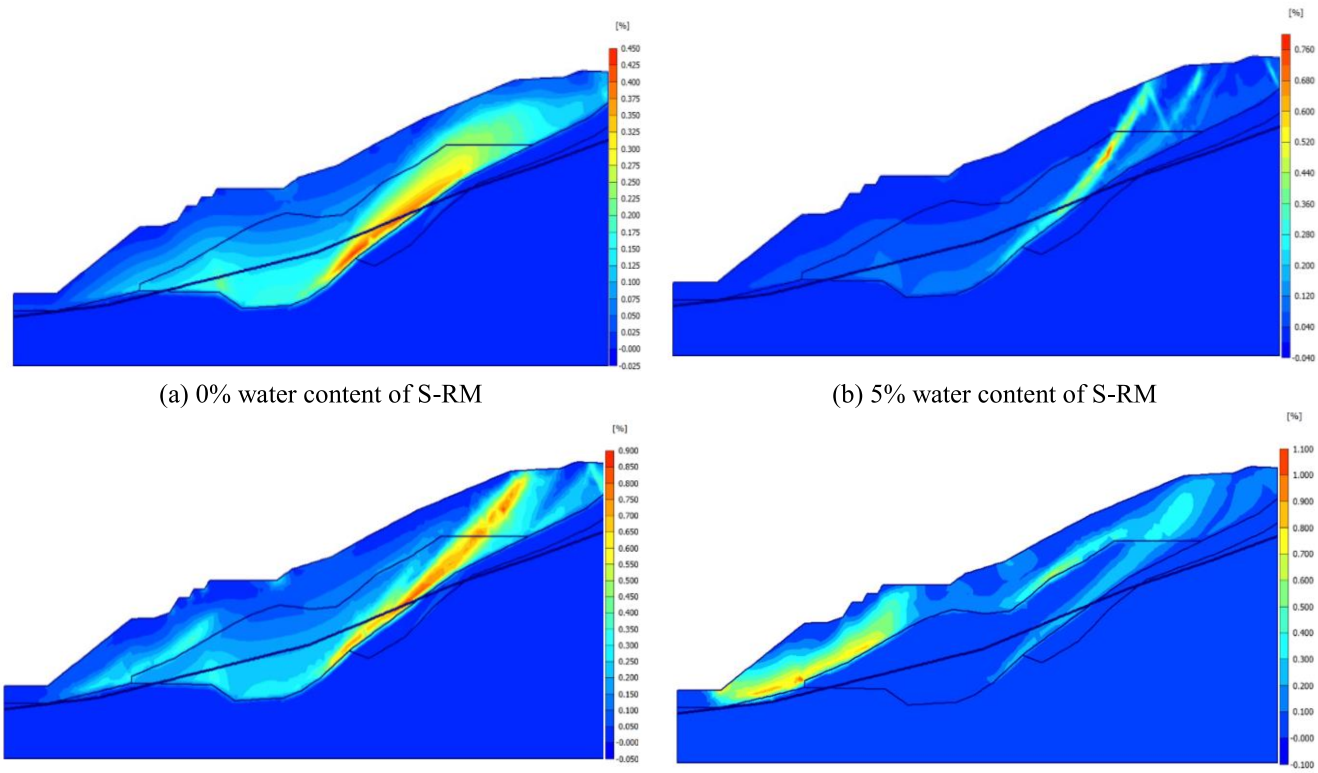

(a) 0% water content of S-RM

(b) 5% water content of S-RM

(c) 10% water content of S-RM

(d) 15% water content of S-RM

Fig. 9 The shear strain increment of talus slope with S-RM having different percentages of water content

approximately analyze the stability of the talus slope under rainfall conditions in this numerical test. Fig. 9 shows the shaded pictures of the shear strain increment of the talus slope, and the slip surface is determined by observing the position of the maximum increase in shear strain, while simultaneously taking the influence of underground water conditions into consideration.

In order to accurately determine the evolution of damage, the shear strength reduction method, called the *Phi-c* reduction approach in PLAXIS, is used to calculate

Table 6 Safety factors of Xiaomiaoling talus slope with different values of strength parameters of S-RM

Water content (%)	0	5	10	15
Cohesive force (kPa)	48.8	17.9	16.5	16.1
Internal friction angle (°)	39.6	37.2	27.3	10.2
Safety factor	2.2715	1.7828	1.2895	0.8966

Table 7 Anti-slide pile material data sets for plate in PLAXIS

Parameter	Anti-slide pile
Young's modulus E (kN/m^2)	3×10^7
Axial stiffness per unit width in the out-of-plane direction EA (kN/m)	3.6×10^8
Flexural rigidity per unit width in the out-of-plane direction EI (kN·m^2/m)	4.8×10^8
Weight per unit area W (kN/m/m)	24
Poisson's ratio V	0.15
Pile size $a \times b$ (m) (a is out-of-plane direction)	3×4
Pile length (m)	20

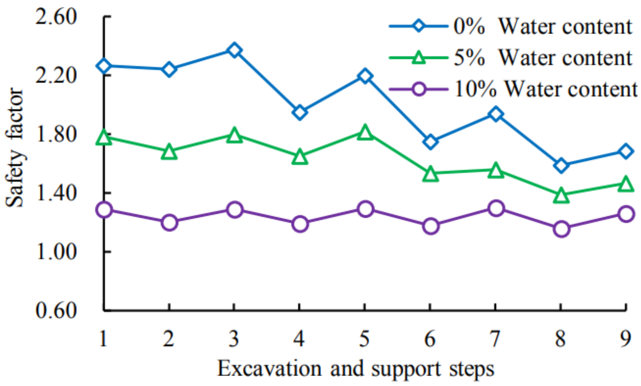

Fig. 10 Safety factors of excavation and support area at different percentages of water content of S-RM and at different stages (the steps 1-9 correspond to the natural state, excavation 1, support 1, excavation 2, support 2, excavation 3, support 3, excavation 4 and support 4)

the safety factor of talus slope.

$$c_f = \frac{c}{f} \tag{3}$$

$$\varphi_f = \tan^{-1}\left(\frac{\tan\varphi}{f}\right) \tag{4}$$

where f is the strength reserve safety coefficient, which is considered as the safety factor when the model of talus slope is in the limit equilibrium state after strength reduction; c_f is the reduced cohesion; and φ_f is the reduced internal friction angle. Table 6 shows the various safety factors of Xiaomiaoling talus slope for different values of strength parameters of S-RM.

The strength parameters of S-RM should ideally be large, exceeding the parameters of colluvial-rubble soil. The bottom shear slip surface of the talus slope is the point of contact between the colluvial-rubble soil and strong weathered sandstone (Fig. 9(a)). The slope itself is very stable with a safety factor of 2.2715. With a decrease in cohesion and internal friction angle, the safety factor reduces further and the slip surface moves up and penetrates the colluvial-rubble soil layer (Fig. 9(b), 9(c)). Although the slip surface is not completely penetrated, it still enters into other parts of the talus slope. In the fourth scenario from Fig. 8(d), it can be easily seen that there are two shear zones: one occurring at the slope toe and the other at the top interface between the S-RM and colluvial-rubble soil. When compared with the first three cases, a new shallow slip surface can be observed, which is almost penetrated while the deep slip surface gradually disappears. In terms of the safety factor, the talus slope has been completely destroyed at the slope toe along the shallow slip surface. The talus slope has a complex and unique spatial distribution and establishing the multistage sliding surface is essential to evaluate the stability of talus slope and formulate a reasonable retaining measure.

5.3 Stability analysis of excavation of talus slope

The excavation and support process of the talus slope was simulated to study the change in talus slope stability during the process. The whole excavation and support process was divided into four steps from top to bottom. During the simulation, the excavation ratios were 1:1.25 (for excavation 1, excavation 2 and excavation 3) and 1:1.5 (for excavation 4). In order to ensure the stability of the talus slope, anti-slide piles were installed at the slope toe after each part of the excavation, and the ongoing excavation was provided support on each terrace level (Fig. 8). The plate element was used to simulate the anti-slide pile in PLAXIS. Some of the simulation parameters of the anti-slide pile can be seen in Table 7.

The numerical simulation of the excavation and support area, denoted by the dotted portion in Fig. 8, is a major part of the analysis. The slope has been destroyed when the water content is 15%, so this situation is not counted in the simulation process. Figure 10 shows the safety factors of excavation and support area during the whole excavation and support process.

It can be observed in Fig. 10 that the excavation of the slope toe reduces the stability of the talus slope, and anti-slide piles are considerably effective in improving the stability of shallow excavation at the same water content. But the effect is gradually weakened with as the excavation proceeds. After the shallow excavation and support (excavation and support 1, 2) is completed, the slip surface moves downward and the slope may be subjected to new slip failure because of the presence of the supporting structure. However, the simulated anti-slide piles 3 and 4 are not buried at a certain depth below the sliding surface as it reduces the efficacy of anti-slide piles.

Under natural conditions, rainfall inevitably changes the water content of talus slope which in turn affects soil strength parameters and interaction of the pile-soil interface. This makes the anti-slide piles shown in Fig. 10 invalid when the water content exceeds a certain value. Hence, it is necessary to pay attention to drainage during the construction of anti-slide piles to prevent the harmful effects of change in water content on excavation slope.

6. Conclusions

The present work consisted of a series of triaxial tests on S-RM samples under different confining pressures (i.e., 100 kPa, 200 kPa and 400 kPa) and having different percentages of water content (i.e., 0%, 5%, 10% and 15%) to investigate the physical and mechanical properties of S-RM. Simultaneously, a simplified geological model of the talus slope was established to compare tits stability with different strength parameters and under different excavation and support processes. The following conclusions can be drawn from this study:

(1) The stress-strain curve of the S-RM sample exhibits a typical non-linear relationship. The samples with low water content began to show weak softening when the strength of samples reached a certain value. When the water content was high, the stress continued to increase with strain, which demonstrated strain hardening behaviour. The strength of samples with different percentages of water content vary greatly even when under same confining pressure. The stress-strain curve is relatively flat with minor fluctuations under low confining pressure. However, under high confining pressure, the local stress exceeds the contact strength of particles in the shear process, which causes cusp breakage or particle breakage and then leads to local fluctuations in stress-strain curve.

(2) The strength parameters of S-RM have been gradually declining, predominantly due to increasing water content, but the influence of the percentage of water content on different strength parameters is variable. The reduction in S-RM strength is largely due to the change in cohesive force when the water content is low and the change in internal friction angle when the water content is high. The low limit and high limit water content mainly control the decrease in the magnitude of cohesive force and the internal friction angle respectively.

(3) The safety factor of the talus slope gradually decreases with the decrease in strength parameters of S-RM. Meanwhile, the slip surface moves up and a new shallow slip surface is created between the S-RM and colluvial-rubble soil at slope toe, which transforms the global stability of talus slope into local stability. It has been verified that the strain softening effect of water on the material of the slip surface is essential for inducing instability of the shallow landslide when the water content is high.

(4) The use of anti-slide piles can considerably improve the stability of shallow slope excavations. But for deep excavation and support, the downward movement of the new failure slope surface needs to be noted. The change in water content of the talus slope caused by rainfall may reduce the efficacy of anti-slide piles when the water content reaches a certain critical value, making it necessary to focus on the drainage measures of anti-slide piles to avoid the detrimental effect of water on the excavation slope.

Acknowledgments

We gladly acknowledge the financial support of the National Natural Science Foundation of China (Grant No. 41672273, 41272292) and the technical support of the Guizhou Provincial Department of Transportation towards our research. The Key Laboratory of Geotechnical and Underground Engineering of the Ministry of Education (Tongji University) has also provided a significant amount of support towards this study.

References

Anbazhagan, S., Ramesh, V. and Saranaathan, S.E. (2017), "Cut slope stability assessment along ghat road section of Kolli hills, India", *Nat. Hazards*, **86**(3), 1081-1104. https://doi.org/10.1007/s11069-016-2731-0.

Brandes, H.G., Robertson, I.N. and Johnson, G.P. (2011), "Soil and rock properties in a young volcanic deposit on the island of Hawaii", *J. Geotech. Geoenviron. Eng.*, **137**(6), 597-610. http://dx.doi.org/10.1061/(ASCE)GT.1943-5606.0000453.

Butalia, T.S., Huang, J., Kim, D.G. and Croft, F. (2003), "Effect of moisture content and pore water pressure build on resilient modulus of cohesive soils", *Proceedings of the Symposium on Resilient Modulus Testing for Pavement Components*, Salt Lake City, Utah, U.S.A.

Cabalar, A.F. and Mustafa, W.S. (2015), "Fall cone tests on clay-sand mixtures", *Eng. Geol.*, **192**, 154-165. https://doi.org/10.1016/j.enggeo.2015.04.009.

Cen, D.F., Huang, D. and Ren, F. (2017), "Shear deformation and strength of the interphase between the soil-rock mixture and the benched bedrock slope surface", *Acta Geotech.*, **12**(2), 391-413. https://doi.org/10.1007/s11440-016-0468-2.

Chang, W.J. and Phantachang, T. (2016), "Effects of gravel content on shear resistance of gravelly soils", *Eng. Geol.*, **207**(3), 78-90. https://doi.org/10.1016/j.enggeo.2016.04.015.

Dimitrova, R.S. and Yanful, E.K. (2012), "Factors affecting the shear strength of mine tailings/clay mixtures with varying clay content and clay mineralogy", *Eng. Geol.*, **125**(1), 11-25. https://doi.org/10.1016/j.enggeo.2011.10.013.

DL/T5356 (2006), "Code for coarse-grained soil tests for hydropower and water conservancy engineering", Professional Standards Compilation Group of People's Republic of China, China Water Power Press, Beijing, China.

Fei, K. (2016), "Experimental study of the mechanical behavior of clay-aggregate mixtures", *Eng. Geol.*, **210**, 1-9. https://doi.org/10.1016/j.enggeo.2016.05.011.

Huang, S.L., Ding, X.L., Zhang, Y.T. and Cheng, W. (2015), "Triaxial test and mechanical analysis of rock-soil aggregate sampled from natural sliding mass", *Adv. Mater. Sci. Eng.*, 1-14. http://dx.doi.org/10.1155/2015/238095.

Jiang, X.G., Cui, P. and Ge, Y.G. (2015), "Effects of fines on the strength characteristics of mixtures", *Eng. Geol.*, **198**, 78-86. https://doi.org/10.1016/j.enggeo.2015.09.011.

Kanungo, D.P., Pain, A. and Sharma, S. (2013), "Finite element modeling approach to assess the stability of debris and rock slopes: a case study from the Indian Himalayas", *Nat. Hazards*, **69**(1), 1-24. https://doi.org/10.1007/s11069-013-0680-4.

Li, C.S., Zhang, D., Du, S.S. and Shi, B. (2016), "Computed tomography based numerical simulation for triaxial test of soil-rock mixture", *Comput. Geotech.*, **73**, 179-188. https://doi.org/10.1016/j.compgeo.2015.12.005.

Liu, J., Wei, J.H., Hu, H., Wu, J.M., Sun, S.R. and Kanungo, D.P. (2017), "Research on the engineering geological conditions and stability evaluation of the B2 talus slide at the Jin'an Bridge hydropower station, China", *Bull. Eng. Geol. Environ.*, **77**(1), 105-125. https://doi.org/10.1007/s10064-017-1005-8.

Liu, Z.Q., Huang, H.W. and Xue, Y.D. (2009), "The application of quantitative risk assessment in talus slope risk analysis", *Georisk*, **3**(3), 155-163. https://doi.org/10.1080/17499510902802644.

Mohammadi, S. and Taiebat, H. (2016), "Finite element simulation of an excavation-triggered landslide using large deformation theory", *Eng. Geol.*, **205**, 62-72. https://doi.org/10.1016/j.enggeo.2016.02.012.

Moradi, G., Abdolmaleki, A., Soltani, P. and Ahmadvand, M. (2018), "A laboratory and numerical study on the effect of geogrid-box method on bearing capacity of rock-soil slopes", *Geomech. Eng.*, **14**(4), 345-354. https://doi.org/10.12989/gae.2018.14.4.345.

Sun, S.R., Xu, P.L., Wu, J.M., Wei, J.H., Fu, W.G., Liu, J. and Kanungo, D.P. (2014), "Strength parameter identification and application of soil-rock mixture for steep-walled talus slopes in southwestern China", *Bull. Eng. Geol. Environ.*, **73**(1), 123-140. https://doi.org/10.1007/s10064-013-0524-1.

Tan, X., Konietzky, H. and Chen, W. (2016), "Numerical simulation of heterogeneous rock using discrete element model based on digital image processing", *Rock Mech. Rock Eng.*, **49**(12), 4957-4964. https://doi.org/10.1007/s00603-016-1030-0.

Vallejo, L.E. (2001), "Interpretation of the limits in shear strength in binary granular mixtures", *Can. Geotech. J.*, **38**(5), 1097-1104. https://doi.org/10.1139/t01-029.

Wang, S.L., Xu, W.Y., Shi, C. and Zhang, Q. (2014), "Numerical simulation of direct shear tests on mechanical properties of talus deposits based on self-adaptive PCNN digital image processing", *J. Central South Univ.*, **21**(7), 2904-2914. https://doi.org/10.1007/s11771-014-2256-1.

Wang, Y. and Li, X. (2014), "Experimental study on cracking damage characteristics of a soil and rock mixture by UPV testing", *Bull. Eng. Geol. Environ.*, **74**(3), 775-788. https://doi.org/10.1007/s10064-014-0673-x.

Wang, Y., Li, X. and Zheng, B. (2017), "Stress-strain behavior of soil-rock mixture at medium strain rates–Response to seismic dynamic loading", *Soil Dyn. Earthq. Eng.*, **93**, 7-17. https://doi.org/10.1016/j.soildyn.2016.10.020.

Wang, Y., Li, X., Zheng, B., Zhang, B. and Wang, J.B. (2015), "Real-time ultrasonic experiments and mechanical properties of soil and rock mixture during triaxial deformation", *Geotech. Lett.*, **5**, 281-286. http://dx.doi.org/10.1680/jgele.15.00131.

Xu, M., Song, E.X. and Cao, G.X. (2009), "Compressibility of broken rock-fine grain soil mixture", *Geomech. Eng.*, **1**(2), 169-178. https://doi.org/10.12989/gae.2009.1.2.169.

Xu, W.J., Hu, R.L. and Tan, R.J. (2007), "Some geomechanical properties of soil-rock mixtures in the Hutiao Gorge area, China", *Geotechnique*, **57**(3), 255-264. http://dx.doi.org/10.1680/geot.2007.57.3.255.

Xu, W.J., Li, C.Q. and Zhang, H.Y. (2015), "DEM analyses of the mechanical behavior of soil and soil-rock mixture via the 3D direct shear test", *Geomech. Eng.*, **9**(6), 815-827. http://dx.doi.org/10.12989/gae.2015.9.6.815.

Xu, W.J., Xu, Q. and Hu, R.L. (2011), "Study on the shear strength of soil-rock mixture by large scale direct shear test", *Int. J. Rock Mech. Min. Sci.*, **48**(8), 1235-1247. https://doi.org/10.1016/j.ijrmms.2011.09.018.

Xu, W.J., Yue, Z.Q. and Hu, R.L. (2008), "Study on the mesostructure and mesomechanical characteristics of the soil–rock mixture using digital image processing based finite element method", *Int. J. Rock Mech. Min. Sci.*, **45**(5), 749-762. https://doi.org/10.1016/j.ijrmms.2007.09.003.

Zhang, H.Y., Xu, W.J. and Yu, Y.Z. (2016a), "Numerical analysis of soil-rock mixture's meso-mechanics based on biaxial test", *J. Central South Univ.*, **23**(3), 685-700. https://doi.org/10.1007/s11771-016-3114-0.

Zhang, H.Y., Xu, W.J. and Yu, Y.Z. (2016b), "Triaxial tests of soil-rock mixtures with different rock block distributions", *Soils Found.*, **56**(1), 44-56. https://doi.org/10.1016/j.sandf.2016.01.004.

Zhong, S.Q., Zhong, M., Wei, C.F., Zhang, W.H. and Hu, F.N. (2016), "Shear strength features of soils developed from purple clay rock and containing less than two-millimeter rock fragments", *J. Mountain Sci.*, **13**(8), 1464-1480. https://doi.org/10.1007/s11629-015-3524-8.

Zhou, Z., Yang, H., Xing, K. and Gao, W.Y. (2018), "Prediction models of the shear modulus of normal or frozen soil-rock mixtures", *Geomech. Eng.*, **15**(2), 783-791. https://doi.org/10.12989/gae.2018.15.2.783.

CC